The 8th Pacific Rim International Congress on Advanced Materials and Processing
Edited by: Fernand Marquis
TMS (The Minerals, Metals & Materials Society), 2013

MECHANICAL PROPERTIES OF LOW-COST BETA-TYPE Ti-Mn ALLOYS FABRICATED BY METAL INJECTION MOLDING

Ken Cho[1], Mitsuo Niinomi[1], Masaaki Nakai[1], Junko Hieda[1], Pedro Fernandes Santos[2], Yoshinori Itoh[3], Masahiko Ikeda[4]

[1]Institute for Materials Research, Tohoku University; Sendai 980-8577, Japan
[2]Department of Metallurgy, Materials Science, and Materials Processing, Tohoku University; Sendai 980-8579, Japan
[3]Industrial Research Institute of Shizuoka Prefecture; Hamamatsu 431-2103, Japan
[4]Faculty of Chemistry, Materials and Bioengineering, Kansai University, Suita 564-8680, Japan

Keywords: β-type Ti alloys, Ti-Mn alloy, low-cost Ti alloy, metal injection molding

Abstract

Ti-10Mn and Ti-14Mn alloys were fabricated by metal injection molding method. Their microstructures and mechanical properties, including tensile properties, Young's modulus, and hardness, were investigated as functions of sintering temperature.
The microstructures of the sintered Ti-10Mn and Ti-14Mn alloys have strong dependence on sintering temperature. Relative densities and grain diameters of the sintered Ti-10Mn and Ti-14Mn alloys increase with increasing sintering temperature. Moreover, all Ti-10Mn and Ti-14Mn alloys sintered at 1373 K, 1423 K, and 1473 K consist of a β phase and a needle-like α phase, whereas Ti-14Mn alloys sintered at 1273 K and 1323 K consist of only a β phase.
The tensile strengths of the sintered Ti-10Mn and Ti-14Mn alloys archive a maximum of 860 MPa and 886 MPa, respectively. However, elongation of the sintered Ti-10Mn and Ti-14Mn alloys are approximately 5% and 1%, respectively. Ti-14Mn alloy sintered at 1273 K shows the lowest Young's modulus (76 GPa) among all the sintered Ti-10Mn and Ti-14Mn alloys. The Vickers' hardness of the sintered Ti-10Mn alloys is almost constant at approximately 320 Hv. On the other hand, the Vickers hardness of the sintered Ti-14Mn alloys increases from approximately 300 Hv to 370 Hv with increasing the sintering temperature from 1273 K to 1473 K. The tensile properties of the sintered Ti-10Mn and Ti-14Mn alloys are poorer than that of Ti-6Al-4V ELI alloy; the ductility in particular is much lower. However, the Young's modulus and hardness of the sintered Ti-10Mn and Ti-14Mn alloys are lower and higher, respectively, than commercial Ti-6Al-4V ELI alloy.

Introduction

Commercially pure Ti (CP-Ti) and (α+β)-type Ti-6Al-4V ELI (mass%, Ti64 ELI) alloy have been widely used for metallic materials for biomedical applications, including artificial hip joints [1], spinal fixation devices [2], and dental implant devices [3]. However, the Young's modulus of CP-Ti and Ti64 ELI alloy is much higher than that of cortical bone. This mismatch between the Young's moduli of cortical bone and that of these implant devices leads to stress shielding, resulting in bone absorption and degradation of bone quality [4]. Therefore, β-type Ti alloys, including Ti-29Nb-13Ta-4.6Zr alloy (mass%, TNTZ) [5] and Ti-35Nb-7Zr-5Ta alloy (mass%, TNZT) [6] have been developed as Ti alloys, each with a low Young's modulus, to overcome this major problem. The Young's modulus of TNTZ is approximately 60 GPa [7], which is much closer to that of the cortical bone (10–30 GPa) [8] than that of Ti64 ELI alloy (110 GPa) [7].

Because of its low Young's modulus and good balance of strength and ductility, β-type Ti alloys such as TNTZ are expected to replace Ti64 ELI alloy as metallic biomaterials.
However, limited availability of alloying elements for these β-type Ti alloys such as niobium (Nb) and tantalum (Ta) is significant concern. Therefore, it is required to develop new β-type titanium alloys containing abundant and less toxic alloying elements. Because of its prevalence, manganese (Mn) is a strong candidate for use as an alloying element of new β-type Ti alloys; significant amounts of manganese nodules and manganese crust exist on the ocean bottom. Moreover, toxicity of Mn is lower than that of V. Therefore, Mn was selected as a β-stabilizer to develop new β-type Ti alloys in this study.
For Ti-Mn binary alloys, an (α+β)-type Ti-8Mn alloy has been developed and standardized for AMS 4908. However, there have been few studies of β-type Ti-Mn alloys with high Mn content (>10 mass%). In this study, β-type Ti-Mn alloys were fabricated by metal injection molding (MIM) method, which is a near-net-shape process. The MIM method is expected to become a common fabrication process to reduce the production costs of biomedical devices fabricated with Ti alloys. The microstructures and mechanical properties, including tensile properties, Young's modulus, and hardness were investigated as a function of sintering temperature.

Experimental Procedures

Material Preparation

Gas-atomized pure Ti powder and fine Mn powder were used as raw materials in this study. Figure 1 and Table I show typical scanning electron microscope (SEM) images and chemical compositions, respectively, of the Ti and Mn powders. The particle size of the raw Ti and Mn powders was less than 45 μm. The Ti-Mn alloys were designed by varying the amount of Mn in Ti alloy with 10 and 14 mass% compositions. The Ti and Mn powders were premixed for 3.6 ks in a pot mill within an argon-filled polyethylene pot. The powder mixtures were then kneaded with a binder by means of a pressure-type kneading machine at 443 K for 8.1 ks. The compounds obtained were crushed and screened to obtain particles with diameters 2–8 mm for the injection molding feedstock. The feedstock was then injection-molded into rectangular and dog-bone-shaped specimens. Figure 2 shows the geometry of (a) rectangular and (b) dog-bone-shaped specimens. The rectangular specimens were prepared for analyzing the chemical compositions.

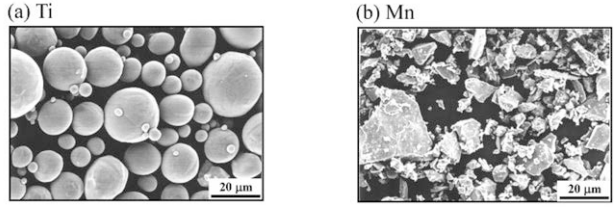

Figure 1. Typical SEM images of (a) Ti power and (b) Mn power.

Table I. Chemical compositions of Ti and Mn powders.

Powder	Fe	O	C	Ti	Mn
Ti	0.044	0.130	0.008	Bal.	-
Mn	0.001	0.770	0.002	-	Bal.

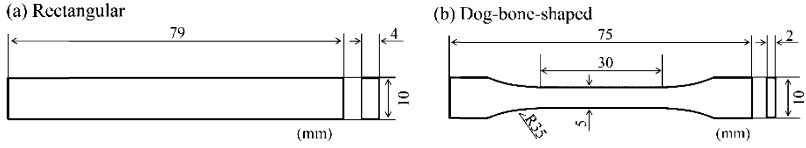

Figure 2. Geometry of (a) rectangular and (b) dog-bone-shaped specimens.

The dog-bone-shaped specimens were prepared for evaluation of relative densities, microstructures, and mechanical properties. After the injection molding, extraction debinding with a vaporized solvent, which was conducted at 343 K for 21.3 ks in n-hexane, was used to partially remove the binder. Following this treatment, sintering was performed at 1273 K, 1324 K, 1373 K, 1423 K, and 1473 K for 28.8 ks in vacuum.

Material Characterization

The chemical compositions of the sintered Ti-Mn alloys were analyzed by inductively coupled plasma optical emission spectroscopy (for Ti and Mn) and the infrared absorption method (for O and C). For analyzing the chemical compositions, 500 μm of the surface layer of the rectangular specimens was removed by mechanically. The densities of the sintered Ti-Mn alloys were measured by an automated densimeter. The relative densities were estimated from the theoretical density (Ti-10Mn: 4.69 Mg/m^3, Ti-14Mn: 4.77 Mg/m^3). The microstructures of the sintered Ti-Mn alloys were evaluated by optical microscope (OM) observation. For the OM observation, the specimens were etched using a 5% HF + 6% HNO_3 etching solution after wet-polishing using waterproof emery papers of up to #800 grit and buff-polishing using 3 μm and 1 μm diamond and colloidal SiO_2 suspension, respectively. The phase constituents of the sintered Ti-Mn alloys were investigated using an X-ray diffraction (XRD) analysis. The XRD analyses were carried out using a Cu target with an operation voltage of 40 kV and a tube current of 40 mA.

Mechanical Tests

The tensile properties of the sintered Ti-Mn alloys were evaluated using an Instron-type testing machine with a cross-head speed of 8.33×10^{-6} $m \cdot s^{-1}$ at room temperature in air. The Young's moduli of the sintered Ti-Mn alloys were estimated from the slope of the elastic region in the stress-strain curves, which were observed by the tensile test. The hardness measurements were carried out using a micro-Vickers hardness tester with a load of 0.9807 N.

Results and Discussion

Material Characterization

Table II shows the chemical compositions of the Ti-10Mn and Ti-14Mn alloys sintered at 1373 K. The actual amounts of Mn in the sintered Ti-10Mn and Ti-14Mn alloys, 9.49 and 13.4 mass%, respectively, are less than the nominal amounts. However, the differences between the nominal and actual amounts are insignificant. The amounts of oxygen in the sintered Ti-10Mn and Ti-14Mn alloys are 0.234 and 0.274 mass%, respectively. These high amounts of oxygen are enough to cause solid solution strengthening for the Ti alloys. Figure 3 shows the relative density of the sintered Ti-10Mn and Ti-14Mn alloys as a function of sintering temperature. As shown in Fig. 3,

Table II. Chemical compositions of Ti-10Mn alloy and Ti-14Mn alloy sintered at 1373 K.

Nominal composition	Ti	Mn	O	C
Ti-10Mn	90.7	9.49	0.234	0.067
Ti-14Mn	86.1	13.4	0.274	0.055

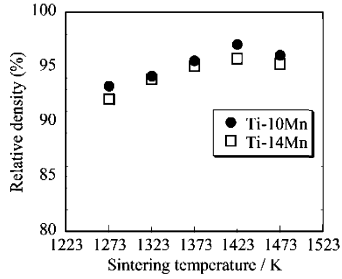

Figure 3. Relative density of sintered Ti-10Mn and Ti-14Mn alloys as a function of sintering temperature.

the relative density of the sintered Ti-10Mn alloys increase from 93% to 97% with increasing the sintering temperature from 1273 K to 1423 K. However, the relative density slightly decreases to 96% at higher sintering temperatures. The relative densities of sintered Ti-14Mn alloys denote same tendency of that of sintered Ti-10Mn alloys. The relative densities of the Ti-14Mn alloys first increase from 92% to 96% with increasing sintering temperature and then slightly decrease to 95%. These results indicate that the porosities of the sintered Ti-Mn alloys increase with increasing sintering temperature. The decreasing of the relative densities in Ti-10Mn and Ti-14Mn alloys sintered at 1473 K is due to evaporation of Mn from the specimen surfaces, which is caused by high temperature sintering. Because of this evaporation of Mn, actual amounts of Mn in the specimen surfaces are smaller than those in the center parts of the specimen.

Figure 4 shows typical OM images of the sintered Ti-10Mn and Ti-14Mn alloys. As shown in Fig. 4, the sintered alloys have equiaxed grains. The grain diameters of the sintered Ti-10Mn and Ti-14Mn alloys increase with increasing sintering temperature because of the grain coarsening that occurred during sintering. Also, fine needle-like structures are found in the equiaxed grains of the sintered Ti-10Mn alloys regardless of the sintering temperature. On the other hand, only the Ti-14Mn alloy sintered at 1473 K has the needle-like structures in the equiaxed grains. However, small amounts of these structures are observed near the grain boundaries of the equiaxed grains in the Ti-14Mn alloys sintered at 1373 K and 1423 K. Figure 5 shows typical XRD profiles of the Ti-10Mn and Ti-14Mn alloys sintered at 1373 K. Diffraction peaks of β (110), β (200), β (211), α (100), α (002), α (102), α (110), α (103), α (112), and α (201) are detected in the sintered Ti-10Mn alloys. On the other hand, only the diffraction peaks of β (110), β (200), and β (211) are detected in the sintered Ti-14Mn alloys. These results indicate that the equiaxed grains present in the sintered Ti-10Mn and Ti-14Mn alloys are β phase and the needle-like structures observed in the equiaxed grains of the sintered Ti-10Mn alloys are α phase. Moreover, although the XRD profile of the sintered Ti-14Mn alloy does not show any diffraction peaks of α phase, the small amount of needle-like structures observed near the grain boundaries of the equiaxed grains sintered at 1373 K and 1423 K are estimated to be α phase, whereas the Ti-14Mn alloys sintered at 1273 K and 1323 K are estimated to consist of a single β phase.

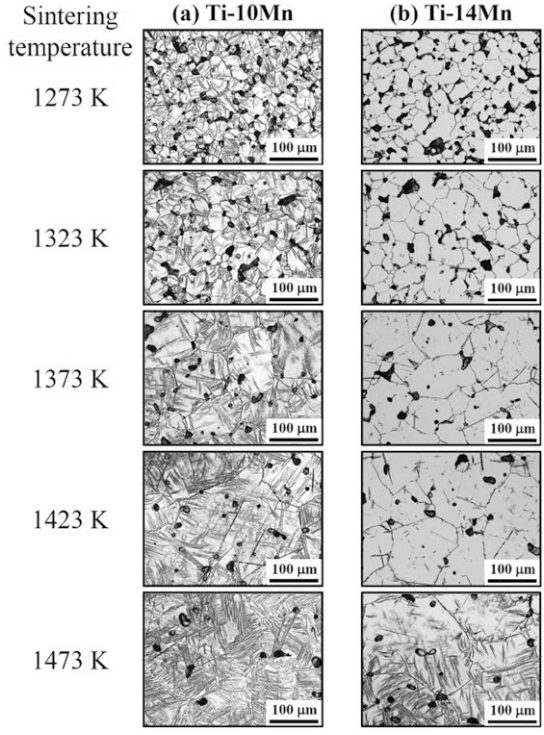

Figure 4. Typical OM images of sintered (a) Ti-10Mn alloys and (b) Ti-14Mn alloys.

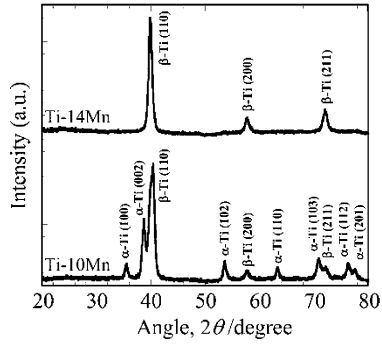

Figure 5. Typical XRD profiles of Ti-10Mn and Ti-14Mn alloys sintered at 1373 K.

Mechanical Properties

Figure 6 shows the tensile strengths, σ_B, 0.2% proof stresses, $\sigma_{0.2}$, and elongations of the sintered (a) Ti-10Mn alloys and (b) Ti-14Mn alloys. As shown in Fig. 6 (a), the tensile strength of the Ti-10Mn alloy sintered at 1273 K is 806 MPa, which then increases to 905 MPa with increasing the sintering temperature to 1423 K. However, the tensile strength decreases to 854 MPa with increasing the sintering temperature to 1473 K. The tensile strengths of the sintered Ti-14Mn alloys are somewhat lower than those of the sintered Ti-10Mn alloys. This is because the volume fractions of the needle-like α phase in the sintered Ti-14Mn alloys are lower than those in the sintered Ti-10Mn alloys, especially the Ti-14Mn alloys sintered at 1273 K and 1323 K, which consist of a single β phase. Moreover, as with the increasing relative density, the tensile strengths of the sintered Ti-10Mn and Ti-14Mn alloys increase with increasing sintering temperature. These results indicate that tensile strength depends on porosity. The 0.2% proof stresses of the sintered Ti-10Mn alloys are approximately 90% of the tensile strength. Such high 0.2% proof stresses are likely due to the low ductility. The elongations of the sintered Ti-10Mn alloys are approximately 5%. Moreover, because fracture of the Ti-14Mn alloys sintered at 1373 K, 1423 K, and 1473 K occurs in the elastic region because of the low elongations (lower than 1%), it can't evaluate the 0.2% proof stresses of these sintered Ti-14Mn alloys. This low ductility of the sintered Ti-10Mn and Ti-14Mn alloys is caused by solid solution strengthening due to oxygen.

The Young's moduli of the sintered Ti-10Mn and Ti-14Mn alloys estimated from the slope of the elastic region in the stress-strain curves are shown in Fig. 7 as a function of sintering temperature. The Ti-14Mn alloy sintered at 1273 K shows the lowest Young's modulus (76 GPa) among all the sintered Ti-10Mn and Ti-14Mn alloys. The Young's moduli of the sintered Ti-10Mn and Ti-14Mn alloys increase from 83 GPa and 76 GPa to 91 Ga and 98 GPa, respectively, with increasing sintering temperature. Wang has reported that the Young's modulus of porous materials increases with decreasing relative density [9]. The current study suggests that the increase in the Young's moduli of the sintered Ti-10Mn and Ti-14Mn alloys is caused by a decrease in the relative density. In other words, the Young's moduli of the sintered Ti-10Mn and Ti-14Mn alloys increase with deceasing porosity. It is well known that the Young's modulus of metallic materials mainly depends on phase constituents. The OM images (Fig. 4) of the sintered Ti-10Mn and Ti-14Mn alloys indicate that the volume fractions of the needle-like α phase of the sintered Ti-10Mn and Ti-14Mn alloys are significantly different. On the other hand, the differences in the Young's moduli of the sintered Ti-10Mn and Ti-14Mn alloys are insignificant. These results suggest that the Young's modulus is much more dependent on porosity than on phase constituents.

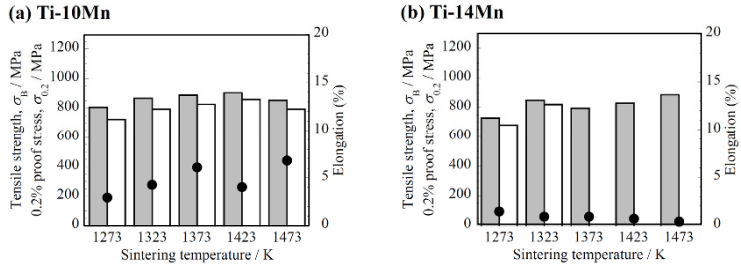

Figure 6. Tensile properties of sintered (a) Ti-10Mn alloys and (b) Ti-14Mn alloys.

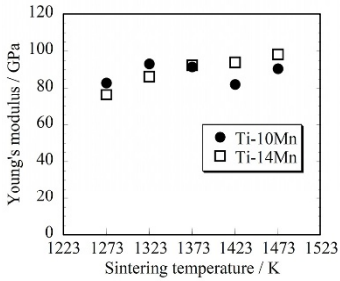

Figure 7. Young's moduli of sintered Ti-10Mn and Ti-14Mn alloys as a function of sintering temperature.

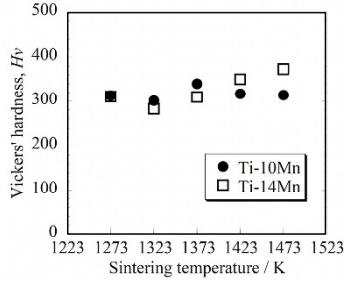

Figure 8. Vickers' hardness of sintered Ti-10Mn and Ti-14Mn alloys as a function of sintering temperature.

Figure 8 shows the Vickers' hardness of the sintered Ti-10Mn and Ti-14Mn alloys as a function of sintering temperature. As shown in Fig. 8, the Vickers' hardness of the sintered Ti-10Mn alloys is almost constant at approximately 320 Hv. On the other hand, the Vickers' hardness of the sintered Ti-14Mn alloys increases from approximately 300 Hv to 370 Hv with increasing the sintering temperature from 1273 K to 1473 K. Although the sintered Ti-10Mn alloys consist of a β phase with a needle-like α phase regardless of the sintering temperature, the phase constituents of the sintered Ti-14Mn alloys change from a single β phase to a β phase with a needle-like α phase with increasing the sintering temperature from 1373 K to 1473 K.

Evaluation of the mechanical properties shows that the tensile properties of the sintered Ti-10Mn and Ti-14Mn alloys are poorer than those of Ti64 ELI alloy, which is the most widely used Ti alloy for biomedical applications. The ductility in particular is much lower than that of Ti64 ELI alloy. However, the Young's modulus and hardness are lower and higher, respectively, than Ti64 ELI alloy. These results indicate that the Ti-Mn alloys have the potential to become a new β-type Ti alloy to replace Ti64 ELI alloy.

Conclusions

1. The relative densities and grain diameters of the sintered Ti-10Mn and Ti-14Mn alloys increase with increasing sintering temperature.
2. All the Ti-10Mn and Ti-14Mn alloys sintered at 1373 K, 1423 K, and 1473 K consist of a β phase with a needle-like α phase. On the other hand, Ti-14Mn alloys sintered at 1273 K and 1323 K consist of only a single β phase.
3. The tensile strengths of the sintered Ti-10Mn and Ti-14Mn alloys achieve a maximum value of 860 MPa and 886 MPa, respectively. However, the elongations of the sintered Ti-10Mn and Ti-14Mn alloys are approximately 5% and 1%, respectively.
4. The Ti-14Mn alloy sintered at 1273 K shows the lowest Young's modulus (76 GPa) among all the sintered Ti-10Mn and Ti-14Mn alloys.
5. The Vickers' hardness of the sintered Ti-10Mn alloys is almost constant at approximately 320 Hv. On the other hand, the Vickers' hardness of the sintered Ti-14Mn alloys increases from approximately 300 Hv to 370 Hv with increasing the sintering temperature from 1273 K to 1473 K.

Acknowledgements

This study was supported in part by Grant-in-Aid for Scientific Research (A) No.24246111 and Grant-in-Aid for Young Scientists (B) No. 25820367 from the Japan Society for the Promotion of Science (JSPS), the interuniversity cooperative research program "Innovation Research for Biosis-Abiosis Intelligent Interface" from the Ministry of Sports, Culture, and Education, Japan, and Inamori Grants from the Inamori Foundation.

References

1. M. Semlitsch, "Titanium alloys for hip joint replacements," *Clinical Materials*, 2 (1987), 1-13.
2. F. B. Christensen, M. Dalstra, F. Sejling, S. Overgaard and C. Bünger, "Titanium-alloy enhances bone-pedicle screw fixation: mechanical and histomorphometrical results of titanium-alloy versus stainless steel," *European Spine Journal*, 9 (2000), 97-103.
3. M. Taira, J. B. Moser and E. H. Greener, "Studies of Ti alloys for dental castings," *Dental Materials*, 5 (1989), 45-50.
4. R. Huiskes, H. Weinans and B. van Rietberge, "The relationship between stress shielding and bone resorption around total hip stems and the effects of flexible materials," *Clinical Orthopaedics and Related Research*, 274 (1992), 124-134.
5. D. Kuroda, M. Niinomi, M. Morinaga, Y. Kato and T. Yashiro, "Design and mechanical properties of new β type titanium alloys for implant materials," *Materials Science and Engineering: A*, 243 (1998), 244-249.
6. Y. L. Hao, S. J. Li, S. Y. Sun, C. Y. Zheng, Q. M. Hu and R. Yang, "Super-elastic titanium alloy with unstable plastic deformation," *Applied Physics Letters*, 87 (2005), 091906/1-3.
7. T. Akahoria, M. Niinomia, H. Fukuib, M. Ogawac and H. Toda, "Improvement in fatigue characteristics of newly developed beta type titanium alloy for biomedical applications by thermo-mechanical treatments," *Materials Science and Engineering: A*, 25 (2005), 248-254.
8. J. A. Davidson and F. S. Gergette, "State of the art in materials for orthopedic prosthetic devices," *Proceedings of Implant Manufacturing and Materials Technology, Society of Manufacturing Engineers*, Em87-122 (1986), 122-126.
9. J. C. Wang, "Young's modulus of porous materials," *Journal of Materials Science*, 19 (1984), 801-808.